1-1-2020

Accurate Segmentation of Cerebrovasculature from TOF-MRA Images Using Appearance Descriptors

Fatma Taher
Zayed University

Ahmed Soliman
University of Louisville

Heba Kandil
University of Louisville

Ali Mahmoud
University of Louisville

Ahmed Shalaby
University of Louisville

See next page for additional authors

IEEE Access
Multidisciplinary | Rapid Review | Open Access Journal

Received February 27, 2020, accepted March 10, 2020, date of publication March 23, 2020, date of current version June 4, 2020.

Digital Object Identifier 10.1109/ACCESS.2020.2982869

Accurate Segmentation of Cerebrovasculature From TOF-MRA Images Using Appearance Descriptors

FATMA TAHER[1], (Member, IEEE), AHMED SOLIMAN[2], (Member, IEEE), HEBA KANDIL[2,3], (Member, IEEE), ALI MAHMOUD[2], (Member, IEEE), AHMED SHALABY[2], (Member, IEEE), GEORGY GIMEL'FARB[4], (Member, IEEE), AND AYMAN EL-BAZ[2], (Senior Member, IEEE)

[1]College of Technological Innovation, Zayed University, Dubai, United Arab Emirates
[2]Bioengineering Department, University of Louisville, Louisville, KY 40292, USA
[3]Information Technology Department, Faculty of Computer Science and Information, Mansoura University, Mansoura 35516, Egypt
[4]Department of Computer Science, The University of Auckland, Auckland 1010, New Zealand

Corresponding author: Ayman El-Baz (aselba01@louisville.edu)

ABSTRACT Analyzing cerebrovascular changes can significantly lead to not only detecting the presence of serious diseases e.g., hypertension and dementia, but also tracking their progress. Such analysis could be better performed using Time-of-Flight Magnetic Resonance Angiography (ToF–MRA) images, but this requires accurate segmentation of the cerebral vasculature from the surroundings. To achieve this goal, we propose a fully automated cerebral vasculature segmentation approach based on extracting both prior and current appearance features that have the ability to capture the appearance of macro and micro-vessels in ToF–MRA. The appearance prior is modeled with a novel translation and rotation invariant Markov-Gibbs Random Field (MGRF) of voxel intensities with pairwise interaction analytically identified from a set of training data sets. The appearance of the cerebral vasculature is also represented with a marginal probability distribution of voxel intensities by using a Linear Combination of Discrete Gaussians (LCDG) that its parameters are estimated by using a modified Expectation-Maximization (EM) algorithm. The extracted appearance features are separable and can be classified by any classifier, as demonstrated by our segmentation results. To validate the accuracy of our algorithm, we tested the proposed approach on *in-vivo* data using 270 data sets, which were qualitatively validated by a neuroradiology expert. The results were quantitatively validated using the three commonly used metrics for segmentation evaluation: the Dice coefficient, the modified Hausdorff distance, and the absolute volume difference. The proposed approach showed a higher accuracy compared to two of the existing segmentation approaches.

INDEX TERMS Cerebrovascular, segmentation, TOF–MRA.

I. INTRODUCTION

IN medicine, there are some diseases that have complicated natures and should be analyzed deeply in order to provide the patient with the right treatment. Among these diseases that can lead to death, or disability, are the cerebrovascular diseases [1]. These types of diseases commonly occur due to the dysfunction of the blood vessels supplying the brain [2]. There are different kinds of cerebrovascular diseases including aneurysms, strokes, arteriovenous malformation, and carotid stenosis [3]. Hemorrhage, a cerebrovascular disease, is considered a cause for strokes for almost 20% of the cases [4]. Furthermore, cerebrovascular diseases are considered the fifth leading cause of death and disability in the US. For neurosurgeons, analyzing the brain scans manually takes a long time and a lot of effort, especially when tracking a small vessel in the orthogonal view in order to be able to get a better picture of the vascular anatomy [5]. With the aid of bio-engineers and computer engineers, several computer-aided-diagnostic systems have been developed to analyze cerebrovascular structures, taking into consideration that any system needs accurate segmentation of the

The associate editor coordinating the review of this manuscript and approving it for publication was Victor Hugo Albuquerque.

cerebrovasculature from its surroundings, and this is the main motivation behind developing our approach.

Several modalities have been used for noninvasive vascular imaging e.g., computed tomography angiography and magnetic resonance angiography (MRA). Three MRA techniques are commonly used for vascular imaging, namely; the Time-of-Flight MRA (TOF-MRA), phase contrast angiography (PCA), and contrast enhanced MRA. Both TOF-MRA and PCA use flowing blood as an inherent contrast medium, while for contrast enhanced MRA, the circularity system is injected with a contrasting substance. PCA exploits phase changes of transverse magnetization when flowing spins move through a magnetic field gradient. This provides good background signal suppression and can quantify flow velocity vectors for each voxel. TOF-MRA which relies on amplitude differences in longitudinal magnetization between flowing static spins is less quantitative, however, it is fast and provides high contrast images. The fact that it is widely used in clinical practice is another motivation behind our work. An overview of the most recent approaches for vascular segmentation will be given below, focusing on cerebrovascular approaches using MRA which are mainly categorized in literature into scale-space filtering, centerline-based, deformable, statistical, hybrid models, and the deep learning based models.

Multiscale filters improve the curvilinear structures in 3D medical imaging by using multiple scales to convolve an image with Gaussian filters [6]–[9]. Moreover, analyzing the eigenvalues of the Hessian for each voxel determines the 3D structures' local shapes. The output of the multiscale filtering represents a new enhanced image in a manner that makes curvilinear structures look brighter while other components look darker [6]. A multiscale-based approach was proposed by Lacoste *et al.* [9] in which Markov marked point processes are used for extracting coronary arteries in 2D X-ray angiograms. The Coronary vessels are locally modeled as piece-wise linear segments of variable widths, lengths, locations, and orientations. A Markov object process based on a uniform Poisson process is used to extract the centerlines of the vessels. In order to optimize the process, simulated annealing is done by using a reversible Markov chain Monto Carlo technique.

Minimal path centerline-based approaches [10]–[12] formulate the extraction of the centerline, using 2 points as the minimum cost integrated across the path of the centerline. The centerlines of blood vessels were extracted by Güls'un and Tek [10] by computing the graph edge cost in the direction of the minimal path using medialness multiscale filtering. The centerline of the full vessel tree was then extracted using a post processing algorithm based on the centerlines scale and length. Furthermore, Pèchaud *et al.* [11] proposed a framework for extracting the tubular structures automatically from 2D images using the shortest paths. They merged orientation and multiscale optimization for the 4D paths to be propagated on the 2D images, where 4D refers to the combination of scale, space and orientation. Minimal path approaches could result in shortcut problems by tracking a false straight path instead of the true curve. This problem was handled by Zhu and Chung [13] who segmented the coronary arteries using a minimum average-cost path.

For deformable models based segmentation techniques or active contour models, they mainly tend to find an estimate of the blood vessels' boundary surface [14]–[19]. The surface energy is optimized by the evolution of an initial boundary (snake) [20]. This is dependent on the smoothness of the surface, in addition to the image gradients. Zhao *et al.* [21] developed a maximum intensity projection active contour based approach for cerebrovascular segmentation. Their method projects the brain into 2D space where an integrated active contour model is applied, and the output is then converted back into 3D. Although the results of this method were very promising, it is complicated as it requires a lot of projections. To segment complex objects and obtain the energy function, it is preferable to consider both the region information and boundary information. A hybrid level-set have been previously proposed by Zhang *et al.* [22] for brain segmentation. A threshold value was set, which represented the lower gray boundary so the algorithm will only extract parts of image with a gray level that is higher than the defined threshold. However, the used threshold value was constant which cannot fit different intensity distributions. Hong *et al.* [23] proposed a localized hybrid level-set that calculates the dynamic threshold locally for the targeted object in the image. Their method was found to segment small vessels more effectively but loses the information in the thick parts. Thus, the hybrid level-set was more effective in segmenting thick vessels but not in tiny vessels, whereas the localized hybrid level-set was more effective in extracting tiny vessels [1].

When comparing deformable models to scale space filtering, deformable models give better results, however they might require some human interaction represented in the initialization. Also, it is worth mentioning that deformable models and scale space filtering are slower than statistical methods.

Statistical approaches for extracting blood vessels are automatic, however the accuracy depends on the probability models being involved. The MRA scans can be considered multimodal as the intensities of each region are accompanied with a specific dominant mode of the intensity total marginal probability distribution. For adaptive statistical vascular segmentation approaches, they were introduced by Wilson and Noble [24] for TOF-MRA as well as Chung and Noble [25] for PC-MRA. In [24], the marginal data distribution was represented with a mixture of 2 Gaussians in addition to a uniform component, corresponding respectively to brain tissues, cerebrospinal fluid, and arteries, while Rician distributions were used in [25] instead of Gaussians. Both approaches made use of a conventional expectation maximization (EM) algorithm in order to estimate the parameters of the mixture. The EM algorithm was modified in [24] by using the marginal grey level distribution instead of the actual grey levels. This modification has been commonly used for density estimation [26].

Various hybrid techniques worked on combining the previously mentioned techniques. As an example, Nain *et al.* [27] combined shape information and signal statistics to derive a region-based deformable contour to segment tubes. Furthermore, geometry of surfaces and second order statistics were used by Law and Chung [28] to guide a deformable model surface for the purpose of vascular segmentation in PC-MRA and TOF-MRA. Wen *et al.* [3] proposed a method based on a Rayleigh-Gaussian mixture model. In their method, when analyzing the histogram, many nonvascular voxels are removed, therefore, this problem can be avoided by dividing the voxels based on their region where vascular voxels are in regions with high intensity and non-vascular voxels are found in the low intensity regions. Cao *et al.* [29] proposed a segmentation method that was based on Markov random field and particle swarm optimization algorithms. In addition, a new finite mixture mode with two Gaussian and one Rayleigh distributions used for the intensity histogram of brain tissues in medical image. Forkert *et al.* [4] presented a cerebrovascular segmentation framework from TOF-MRA that combines statistical, deformable and scale-space techniques. In their method, they calculated the vesselness and then used fuzzy logic to combine it with the TOF-MRA data. This was then used to initialize a level-set technique. Their work was extended by Woźniak *et al.* [30] by modifying the vesselness function to include multiscaling in order to handle different vascular sizes. Moreover, Zhao *et al.* [31] proposed a framework for segmenting cerebral vessels from MRA using gradient information and statistics.

Deep learning based models have recently gained a lot of attention as they provide a new trend to extract the features in addition to final classification to provide the final segmentation labels. Kandil *et al.* [32] developed a new 3D convolutional neural network (3D-CNN) based segmentation approach that divides the brain into two compartments, (above, and at and below circle of Willis, CoW), relying on the intensity variations as the blood flow changes to provide an enhanced segmentation. Livne *et al.* [33] used the U-net deep learning framework with energy function computed by a voxel wise sigmoid over the final feature map combined with the Dice coefficient as the loss function to segment blood vessels from MRA scans.

In summary, the above-mentioned overview demonstrates the following limitations:

- Most of the cerebral segmentation approaches are semi-automatic which require user interaction to initialize a vessel of interest, in particular, the deformable based segmentation approaches.
- Some of them developed their approaches based on an assumption the vessels follow tubular shape; this holds for healthy people but not for patients with stenosis or an aneurysm.
- Most of them are developed based on using pre-trained models and did not take into account any features from the given data to make their approach adaptable and not biased to the training data.

To overcome the above-mentioned limitations, we developed a fully automated segmentation approach that takes into account both current and prior appearance models. For prior appearance, we developed a new MGRF model, invariant under translation in the (x, y) plane and under rotations around the z axis, which has the ability to capture the 1^{st} order appearance model as well as the 2^{nd} order appearance model without using any alignment algorithms. For current appearance model, we used the Linear Combination of Discrete Gaussians (LCDG) model to estimate the marginal density of the blood vessels from the MRA data.

II. METHODS

We present a fully automated framework to extract both micro and macro brain blood vessels from MRA images. As demonstrated in Figure 1, the proposed framework consists of the following major steps: (*i*) bias correction and skull stripping, (*ii*) enhancement of vascular contrast and homogeneity, (*iii*) modeling vascular prior appearance using a pairwise, rotation and translation invariant, Markov-Gibbs random field (MGRF), the interaction parameters of which have been analytically estimated from a set of MRA training data, (*iv*) modeling the current appearance using our prior model and LCDG approach, (*v*) initial classification of vascular tissue, and (*vi*) final extraction of the brain vascular system based on 3D connectivity analysis. The proposed framework in Figure 1 avoids many of the shortcomings of the methods presented in the literature. In particular, it does not require any alignment steps because all the proposed models are translation and rotation invariant in the (x, y) plane. Also, the proposed framework is not biased toward the training data, due to its taking into account the current appearance of the MRA data as well as the learned prior appearance model of the cerebral vasculature. Finally, the proposed framework performs well in the presence of inhomogeneities that may exist in MRA images. This is due to its encoding local spatial information using the MGRF model to identify vascular tissue irrespective of large-scale variation in absolute signal intensities. Details of the proposed approach are outlined in the following sections.

- **Basic notations:-**
- Let (x, y, z) denote Cartesian coordinates of points in a finite arithmetic lattice $\mathbf{R} = \{(x, y, z) : x = 0, \ldots, X - 1; y = 0, \ldots, Y - 1, z = 0, \ldots, Z - 1\}$.
- $\mathbf{Q} = \{0, \ldots, Q - 1\}$ denotes a set of gray levels.
- $g : \mathbf{R} \rightarrow \mathbf{Q}$ is a 3D grayscale image.

A. BIAS CORRECTION AND SKULL STRIPPING

Illumination non-uniformity of brain MR images, which is known as bias field, limits the accuracy of the brain tissue segmentation and extraction approaches. These approaches presents a very important step to extract the region of interest for the subsequent segmentation approaches. Therefore, the accurate extraction of the brain requires accounting for the low-frequency intensity non-uniformity or inhomogeneity.

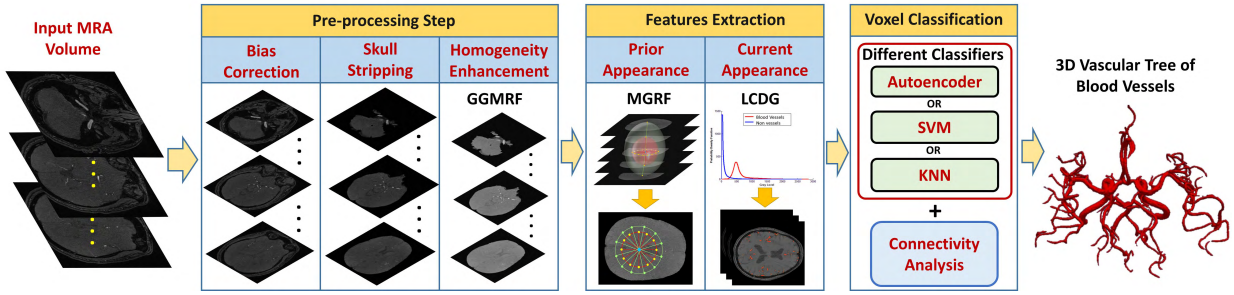

FIGURE 1. The proposed segmentation framework showing the step by step details starting from Pre-processing, feature extraction, voxel classification, and finally the post-processing.

A non-parametric bias correction algorithm [34] was used to reduce any effects of noise and to remove data inconsistencies. Consequently, the brain extraction tool was used to remove the skull and keep the brain tissue only [34].

B. HOMOGENEITY ENHANCEMENT

To enhance the vascular homogeneity in this work, we developed a new 3D Rotational and Translational Invariant Generalized Gauss-Markov random field (RTI-GGMRF) model. This model will be applied after the bias correction and skull stripping step. The main idea of the model is to reduce the signals inconsistencies of the MRA data by estimating the new grey level that minimize the Gibbs energy between the voxel of interest and its neighbors. To ensure the proposed RTI-GGMRF is invariant under rotations and translations, we selected the neighborhood system to be central-symmetric around the voxel of interest (e.g., spherical-neighborhood system) as demonstrated in Figure 2. In order to use the proposed RTI-GGMRF model to estimate the MRA signals that enhance the homogeneity of MRA data, let the gray level values of a volume g be considered as samples from a 3D RTI-GGMRF model [35] with spherically symmetric neighborhood system $(\mathbf{n}_1, \mathbf{n}_2)$. The maximum a posteriori estimates [35] and voxel-wise stochastic relaxation (iterative conditional mode [36]) of voxel values at each location $s \in \mathbf{R}$ are as follows:

$$\widehat{q}(s) = \arg\min_{q} |g(s) - q|^{\alpha} + \rho^{\alpha}\lambda^{\beta} \sum_{r\in\mathbf{n}_1} \eta_1(r)|g(s+r) - q|^{\beta} + \rho^{\alpha}\lambda^{\beta} \sum_{r\in\mathbf{n}_2} \eta_2(r)|g(s+r) - q|^{\beta}] \quad (1)$$

The neighborhood $\mathbf{n}_1$ is located at a unit distance from the central voxel. Similarly, $\mathbf{n}_2$ is the neighborhood located at a double unit distance from the central voxel. η_1 and η_2 are the corresponding RTI-GGMRF potentials, and ρ and λ are scaling factors. The parameter $\beta \in [1.01, 2.0]$ controls the smoothing level (e.g., $\beta = 2$ for smooth vs. $\beta = 1.01$ for noisy edges). The parameter $\alpha \in \{1, 2\}$ determines the Gaussian, $\alpha = 2$, or Laplace, $\alpha = 1$, prior distribution of the estimator.

To enhance the contrast of MRA images, we are proposing to use our former, unsupervised first-order appearance model

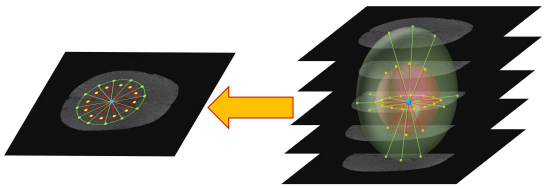

FIGURE 2. A 2D and 3D illustration of the proposed rotational and translational invariant neighborhood system. The center voxel and the neighborhood system are cololred in blue and yellow respectively.

to estimate the marginal grey level distributions of blood vessels and other brain tissues.

An LCDG model with K of dominant modes is given by a sum of C_{p} positively weighted and C_{n} negatively weighted discrete Gaussian components with $C_{\mathrm{p}} \geq K$:

$$P(q) = \sum_{r=1}^{C_{\mathrm{p}}} w_{\mathrm{p},r}\,\psi(q|\theta_{\mathrm{p},r}) - \sum_{l=1}^{C_{\mathrm{n}}} w_{\mathrm{n},l}\,\psi(q|\theta_{\mathrm{n},l}) \quad (2)$$

where $\psi(q|\theta)$ is the discrete Gaussian distribution on $\mathbf{Q}$ with parameter vector $\theta = (\mu, \sigma^2)$ and the weights are constrained to be nonnegative and the the difference between their summation equal 1

The parameters of the LCDG were estimated using the modified expectation-maximization algorithm in [37].

Assuming the positively weighted discrete Gaussian components are ordered such that $\mu_{p,1} \leq \mu_{p,2} \leq \cdots \leq \mu_{p,C_p}$, the marginal distribution of grey levels within brain tissue (grey/white matter) and within blood vessels were calculated as

$$P(q|\text{Brain}) = \frac{1}{\alpha}\sum_{r=1}^{2} w_{\mathrm{p},r}\,\psi(q|\theta_{\mathrm{p},r}) - \sum_{l=1}^{C_{\mathrm{n}}} w_{\mathrm{n},l}\,\psi(q|\theta_{\mathrm{n},l})$$

$$P(q|\text{Vessels}) = \frac{1}{1-\alpha}\sum_{r=3}^{C_{\mathrm{p}}} w_{\mathrm{p},r}\,\psi(q|\theta_{\mathrm{p},r}) - \sum_{l=1}^{C_{\mathrm{n}}} w_{\mathrm{n},l}\,\psi(q|\theta_{\mathrm{n},l}) \quad (3)$$

where $\alpha = \frac{w_{\mathrm{p},1}+w_{\mathrm{p},2}}{\sum_r w_{\mathrm{p},r}}$.

Given these preliminaries, we employed the following algorithm to improve the homogeneity and contrast of MRA images as follows:

1) Choose $\delta > 0$
2) For each MRA volume $g : \mathbf{R} \rightarrow \mathbf{Q}$
   a) For each slice $g_i \subset g$
      i) Estimate parameters of the LCDG model using modified EM algorithm.
      ii) Calculate the empirical marginal distributions of brain tissue $P_i(q|\text{Brain})$ and blood vessels $P_i(q|\text{Vessel})$ using equation 3
   b) Initialize contrast-enhanced image $E : \mathbf{R} \rightarrow \mathbb{R}$
   c) For each $s \in \mathbf{R}$
      i) Solve Eq. 1 for $\widehat{q}(s)$ using gradient descent
      ii) $P_v \leftarrow P_i([\widehat{q}(s) + 0.5]|\text{Vessel})$, where $[\cdot]$ denotes the greatest integer function.
      iii) $P_o \leftarrow P_i([\widehat{q}(s) + 0.5]|\text{Brain})$
      iv) If $P_v \geq P_o$
      $$E(s) \leftarrow \widehat{q}(s) + \delta$$
      else
      $$E(s) \leftarrow \widehat{q}(s) - \delta$$

Note that δ is a "small" value controlling the degree of contrast enhancement; in all our experiments we used $\delta = 1$.

C. ROTATION AND TRANSLATION INVARIANT MGRF-BASED PRIOR CEREBRAL VASCULATURE APPEARANCE MODEL

To develop the proposed learnable MGRF model in a way that it does not require any alignment stage in order to use it to extract cerebral vasculature, the appearance of cerebral vasculature is modeled using a 3D MGRF, having 2D rotational and translational symmetry, with neighborhood system $\mathbf{N}$. As illustrated in Fig. 2, $\mathbf{N}$ is specified by a set of characteristic voxel neighborhoods of the origin $\{\mathbf{n}_\nu : \nu = 1, 2, \ldots, N\}$ and their corresponding Gibbs potentials $\mathbf{V}_\nu$. A characteristic neighborhood $\mathbf{n}_\nu$ is spherically symmetric if and only if it comprises all voxels whose distance from the origin falls within a half-open interval, $\mathbf{n}_\nu = \{r : d_{\min,\nu} \leq ||r|| < d_{\max,\nu}\}$.

Since the MRA appearance of the cerebral vasculature changes from large vessels (bright) to microvessels (less bright), we have to take this effect into account in order to accurately segment cerebral vasculature. To accomplish this we developed the 3D interaction system to be a function in the z (inferior–superior) direction. That is, for each axial slice of the MRA volume there is a corresponding set of Gibbs interaction potentials $\mathbf{V}_\nu(q, q'; z)$, as well as a gray level potential $\mathbf{V}_0(q, q'; z) = \mathbf{V}_0(q; z)$. Note that $\mathbf{V}_0$ represents the estimated potential for the first order prior appearance of the cerebral vasculature and $\mathbf{V}_\nu$ is the pairwise, or second order, prior appearance of the cerebral vasculature.

To identify/learn the proposed MGRF model, we have to estimate the potentials $\mathbf{V}_\nu$ and $\mathbf{V}_0$. Thus, consider a training set of MRA volumes $\mathbf{g} = \{g_1, \ldots, g_T\}$, $T = 20$ in our experiments, and the families of voxel pairs (s, s') where $s \in \mathbf{R}$, $s' = s + r$, and $r \in \mathbf{n}_\nu$. Let $\mathbf{F}_{\nu,t}(q, q'; z)$ be a joint empirical probability distribution of gray level co-occurrences in the training nodules from the image $\mathbf{g}_t$. Also define $\mathbf{F}_{0,t}(q, q'; z) = \mathbf{F}_{0,t}(q; z)$ as the empirical distribution of gray levels.

The MGRF model of the t-th object is specified by the joint Gibbs probability distribution on the sublattice $\mathbf{R}_t = \{s \in \mathbf{R}|g_t(s) \text{ is vasculature}\}$.

$$P_t(q, q') = \frac{1}{Z_t} \exp\left(|\mathbf{R}_t| \sum_{\nu=0}^{N} \left(\rho_{\nu,t} \sum_{z=1}^{Z_t-1} V_{\nu,t}(q, q'; z)\, \mathbf{F}_{\nu,t}(q, q'; z)\right)\right) \quad (4)$$

where $\rho_{\nu,t}$ is the average cardinality of the neighborhood $\mathbf{n}_\nu$ with respect to the sublattice $\mathbf{R}_t$. We make the simplifying assumption that different vascular trees have approximately the same total volume, $|\mathbf{R}_t| = R_{\text{vasc}}$, and the same neighborhood sizes, $\rho_{\nu,t} = \rho_\nu$. For independent samples, the joint probability distribution of gray values for all the training cerebral vasculature is as follows:

$$P_{\mathbf{S}} = \frac{1}{Z} \exp\left(TR_{\text{vasc}} \sum_{\nu=0}^{N} \left(\rho_\nu \sum_{z=1}^{Z-1} V_{\nu,\text{vasc}}(q, q'; z)\, \mathbf{F}_{\nu,\text{vasc}}(q, q'; z)\right)\right) \quad (5)$$

where the marginal empirical distributions of gray levels $\mathbf{F}_{0,\text{vasc}}$ and gray level co-occurrences $\mathbf{F}_{\nu,\text{vasc}}$ describe all the cerebral vasculature from the training set. The potentials are approximated using the analytical approach similar to that in [38].

For computing MGRF energies E_0 and E_ν of the spherically-symmetric pairwise voxel interactions in the training data, note that the energies are equal to the variances of the co-occurrence distributions:

$$E_0(z) = \sum_{q=0}^{Q-1} \mathbf{F}_{0,\text{vasc}}(q; z) \left(\mathbf{F}_{0,\text{vasc}}(q; z) - \frac{1}{Q}\right) \quad (6)$$

$$E_\nu(z) = \sum_{q=0}^{Q-1} \sum_{q'=0}^{Q-1} \mathbf{F}_{\nu,\text{vasc}}(q, q'; z) \left(\mathbf{F}_{\nu,\text{vasc}}(q, q'; z) - \frac{1}{Q^2}\right) \quad (7)$$

The calculated Energies from Eqs. (6 and 7) will be used as discriminatory features that represent the first-order and second-order prior appearance model of the cerebral vasculature.

D. LCDG-BASED CURRENT APPEARANCE MODEL

In addition to the appearance prior that learned from the normalized training data sets that are modeled using the MGRF model, we model the marginal gray level distribution with a dynamic mixture of two distributions for brain blood vessels and other brain tissues, respectively, by using the

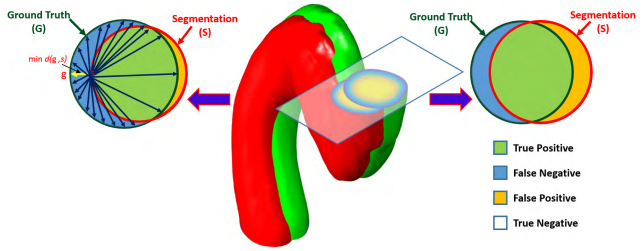

FIGURE 3. Illustration of the Dice coefficient, *(right)*, and the Hausdorff evaluation, *(left)*, metrics. Evaluation is performed in 3D while a 2D cross section is depicted for visualization simplicity.

LCDG model in Eq. 3 to estimate their marginal densities. This modeling will overcome the problems that stem from the visual appearance variations between different subjects, **g**, that will be segmented. These differences can be caused by the changes in patient tissue characteristics, different data acquisition systems that causes non-linear intensity variations, scanner type, and scanning parameters.

E. EXTRACTION OF THE CEREBRAL VASCULATURE

To highlight that the features extracted using the proposed segmentation approach are separable and can be accurately classified/segmented by any classifier algorithm, the extracted prior appearance features and current appearance features were fed into different classifiers (Figure 1), namely, Support Vector Machine (SVM), Neural Network, auto-encoder network followed by softmax decision network, and decision tree. The classifier with the highest accuracy was used (SVM in experiments below). To extract the final segmented cerebral vasculature, the Image Processing Toolbox within Matlab was used to extract the largest connected 3D component from the initial segmentation that was obtained using the the SVM classifier. After assigning a unique label for each individual connected component, a volume and shape-based constraints are applied to select the largest components that satisfy a predefined threshold and tabularity shape conditions.

To summarize, the whole segmentation approach is as follows:

1) Read TOF-MRA volume
2) Apply the bias correction algorithm followed by the skull stripping algorithm as demonstrated in Section II-A.
3) Apply the proposed homogeneity enhancement algorithm as demonstrated in Section II-B.
4) Use Eqs. 6 and 7 to estimate the energy of the first-order and second-order prior appearance.
5) Use Eq. 3 to estimate the probability density for any voxel to be blood vessels ($P(q|\text{Vessels})$) and probability to be other brain tissues ($P(q|\text{Brain})$).
6) Feed the estimated current and prior features to your classifier.
7) Extract Cerebral Vasculature by using the Matlab toolbox to extract the largest connected components.

To Summarize, the proposed method is based on modeling and generating engineered features (some of them depends on training data, e.g., the MGRF Gibbs energy feature), then feed these features to a machine learning classifiers.

F. EVALUATION METRICS

The segmentation results of the proposed blood vessels segmentation framework are evaluated using two types of metrics: area-based similarity metrics and a distance-based error. The area-based similarity indicates the overlap between the segmented area and the ground truth. These types of metrics are crucial for studying area measurements, e.g., total volumes of blood vessels. The distance-based error measures how close the edges of the segmented vessels are to the ground truth. In this paper, we used the Dice coefficient (DC) and absolute vessels volume difference (AVVD) to describe the area-based similarity, while the 95-percentile bidirectional Hausdorff distance (BHD) is used to characterize the distance-based error metric. These evaluation metrics are detailed below.

1) DICE COEFFICIENT (DC)

The Dice coefficient (DC) is used first to evaluate the segmentation accuracy. DC is the most commonly used similarity metric for segmentation evaluation by characterizing the agreement between the segmented (**S**) and the ground truth (**G**) regions by calculating the true positive (*TP*) value, true negative (*TN*) value, false negative (*FN*) value, and false positive (*FP*) value. The *TP* represents the number of positively labeled voxels that are correct; the *FP* is the number of labeled voxels that are classified positively while it is incorrect; the *TN* is the number of negatively labeled voxels that are correct; and the *FN* is the number of negatively labeled voxels that are incorrect. The DC value is calculated using all these values as follow [39]:

$$\text{DC} = \frac{2 \cdot \text{TP}}{2 \cdot \text{TP} + \text{FP} + \text{FN}} \times 100 \tag{8}$$

The calculated value of the DC can have a percentage value in the range 0% to 100%, where 0% means strong dissimilarity and 100% means a perfect similarity. To obtain the ground truth that used in the segmentation evaluation process, an MRA expert delineated the brain vessels.

2) ABSOLUTE VESSELS VOLUME DIFFERENCE (AVVD)

Another area-based metric that is used in this paper for the evaluation of segmentation, in addition to the DC, is the absolute Vessels volume difference (AVVD). The AVVD is the volume difference (percentage), between the output of the segmentation framework, **S**, and the ground truth, **G**, as follows:

$$\text{AVVD}(\mathbf{G}, \mathbf{S}) = \frac{|\mathbf{G} - \mathbf{S}|}{|\mathbf{G}|} \times 100 \tag{9}$$

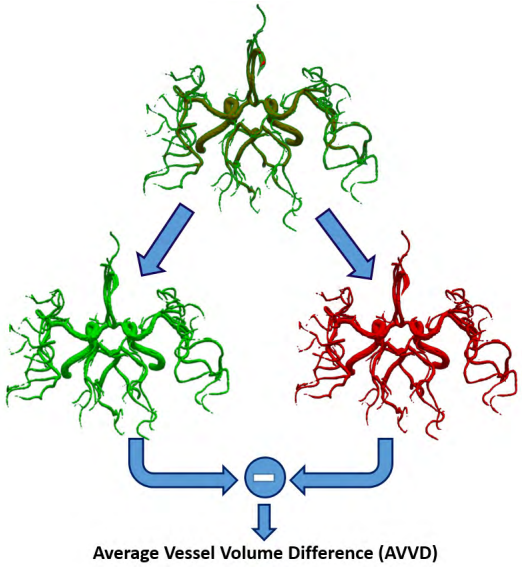

FIGURE 4. Visualization of the average vessel volume difference. The ground truth and the segmented volumes, *in the second row*, colored in green and red respectively.

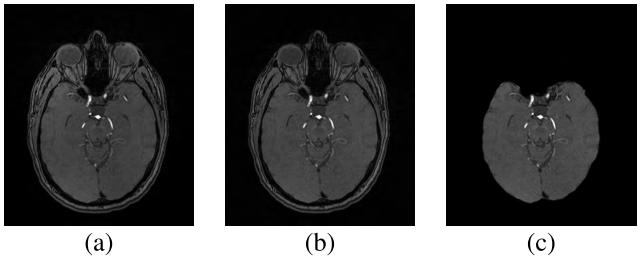

FIGURE 5. Illustration of the pre-processing steps, *(in 2D projection)*: (a) Original axial slice, (b) Output after applying bias correction and homogeneity algorithms, and (c) Output after applying the skull stripping algorithm.

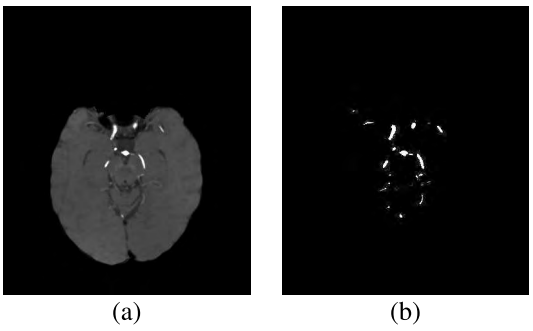

FIGURE 6. Voxel-wise Gibbs energy: (a) 1^{st}-Order Gibbs energy and (b) total Gibbs energy.

where $|\mathbf{G} - \mathbf{S}|$ is the absolute difference between the number of voxels in $\mathbf{G}$ and $\mathbf{S}$, $|\mathbf{G}|$ is the number of voxels in $\mathbf{G}$.

3) BIDIRECTIONAL HAUSDORFF DISTANCE (BHD)

In addition to the DC and AVVD, the distances between $\mathbf{G}$ and $\mathbf{S}$ borders are used as an additional metric to measure the accuracy of the segmentation framework. To measure the

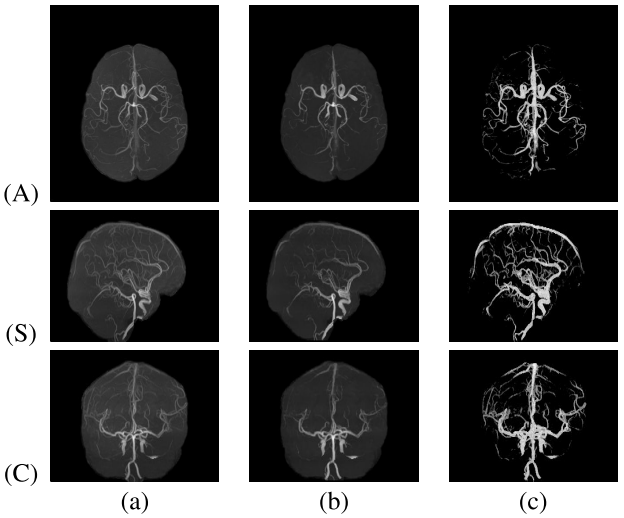

FIGURE 7. Maximum Intensity Projection (MIP) presented on the 2D axial (A), coronal (C), and sagittal (S) planes for visualization. (a) MIP-visualization of original MRA data, (b) MIP-visualization of MRA data after applying bias correction and homogeneity algorithms, and (c) MIP-visualization for the estimated voxel-wise Gibbs energy.

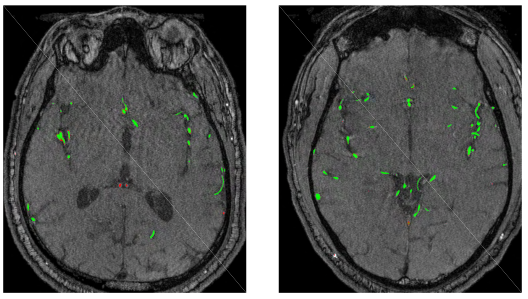

FIGURE 8. A 2D axial projection for the segmentation results from two different subjects using the proposed technique. The true positive, and false negative segmentation's are overlaid with green, and red, respectively.

distance error between the borders of $\mathbf{G}$ and $\mathbf{S}$, we used the bidirectional Hausdorff distance (BHD). The HD from the boarder points of $\mathbf{G}$ to the boarder points of $\mathbf{S}$ is defined as the maximum distance from the border of $\mathbf{G}$ to the nearest point on the border of $\mathbf{S}$ [39], [40]:

$$\mathrm{HD}(\mathbf{G}, \mathbf{S}) = \max_{g \in \mathbf{G}} \{\min_{s \in \mathbf{S}} \{d(g, s)\}\} \tag{10}$$

where g and s denote points of set $\mathbf{G}$ and $\mathbf{S}$ respectively, and $d(g, s)$ is the Euclidean distance between g and s.

The bidirectional Haussdorf distance (BHD) between the segmented region $\mathbf{S}$ and its ground truth $\mathbf{G}$ is defined as:

$$\mathrm{BHD}(\mathbf{G}, \mathbf{S}) = max\{\mathrm{HD}(\mathbf{G}, \mathbf{S}), \mathrm{HD}(\mathbf{S}, \mathbf{G})\} \tag{11}$$

In this paper, we use the 95th-percentile bidirectional Haussdorf distance (BHD) as a metric that measures the segmentation accuracy.

III. EXPERIMENTAL RESULTS

In order to evaluate the performance of the proposed cerebral vasculature segmentation system, it was applied to 270 ToF–MRA data sets which were obtained from the

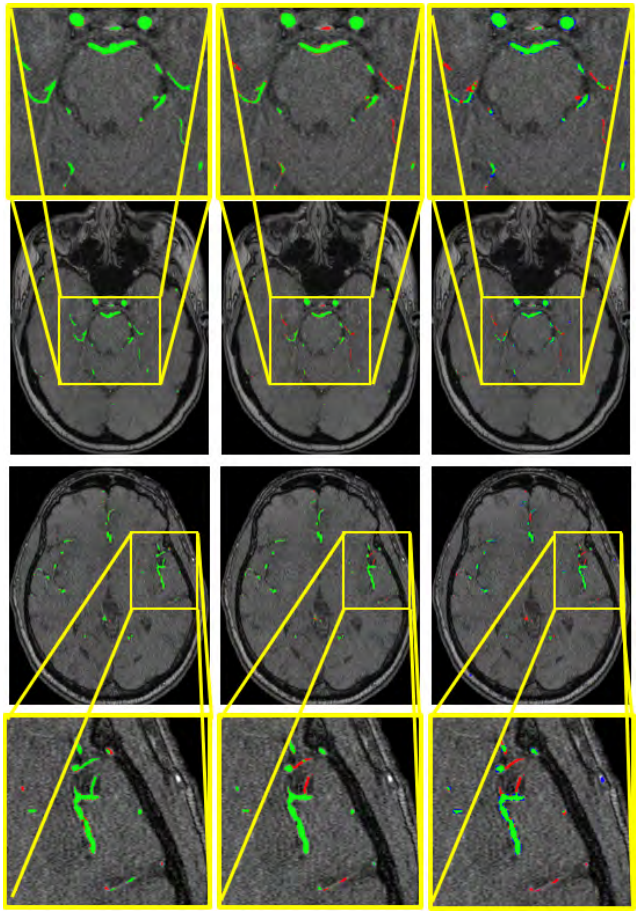

FIGURE 9. Sample of 2D segmentation results, for two different cross sections, *(first and third rows)*, and zooming for selected regions, *(second and fourth rows)*. From left to right, the output segmentation of: proposed method, method by [32], and then [33]. The true positive, false negative, and false positive segmentation's are overlaid with green, red, and blue respectively.

TABLE 1. Comparison between the proposed segmentation framework and other two segmentation techniques.

		Evaluation Metric		
		DC	AVVD	BHD
Global methods	Livne et al. [33]	80.25	16.70	8.85
	CNN method. [32]	83.20	14.80	6.30
	Proposed system	89.10	12.50	5.80
	p-value	0.0001	0.0001	0.0001
Below coW	Livne et al. [33]	83.56	15.83	7.10
	CNN method. [32]	85.30	10.25	7.20
	Proposed system	93.40	8.40	3.20
	p-value	0.0001	0.0001	0.0001
Above coW	Livne et al. [33]	78.30	18.52	9.30
	CNN method. [32]	79.50	16.20	6.10
	Proposed system	82.70	12.10	4.10
	p-value	0.0001	0.0001	0.0001

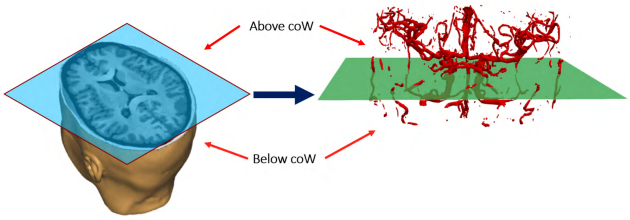

FIGURE 10. 3D visualization of the circle of Willis boundaries in a typical MRA, *(left)*, volume and its corresponding vasculature, *(right)*.

TABLE 2. Comparison between the execution, *(minutes)*, time for the proposed segmentation framework and other two segmentation techniques. The CNN method is reported for the testing phase only.

	Evaluation Metric		
	Livne et al. [33]	CNN [32]	Proposed
Execution Time	5.0	5.9	3.8

FIGURE 11. 3D vasculature visualization of sample output segmentation obtained using the proposed framework for the three different subjects.

University of Pittsburgh, Pennsylvania, USA, through our collaborator in this project. An MRA expert delineated the brain vessels to provide the ground truth that will be used in the evaluation process. The ToF–MRA data were acquired using a 3.0T Trio MRI scanner with a 12-channel phased-array head coil (TR=21.0, TE=3.8, flip angel=22). Each volume has the size of 384 × 448 × 160 with a slice thickness of 0.5 *mm*.

To highlight the role of each step in the proposed segmentation system, we demonstrate in Figure 5 the output of each step for a selected axial cross-section of one subject. As shown in Figure 5(b), the homogeneity and contrast are enhanced by using the proposed GGMRF model. Figure 6 highlights the advantages of using a higher order MGRF model versus using only the 1^{st}-order MGRF model. Another way to visualize our new Gibbs energy and compare it to the original intensity of MRA data is to use maximum intensity projection for the original MRA data and the estimated voxel-wise Gibbs energy of MRA data as demonstrated in Figure 7. It is clear from Figure 6(b) that the estimated voxel-wise energy for the brain vascular system is high compared with the other brain tissues, which encourage us to use the estimated Gibbs energies as separable features to extract brain vascular system from MRA images.

Figure 8 presents the segmentation results on the 2D axial plane for the proposed vasculature segmentation system by using the SVM classifier as it obtained the highest overall accuracy.

To highlight the advantages of the proposed segmentation approach, we compared it with CNN-based segmentation approach proposed by Kandil *et al.* [32] and statistical based segmentation approach proposed by Livne *et al.* [33] (Figure 9). Table 1 shows a comparative evaluation using the aforementioned evaluation metrics, for the obtained 3D segmentation, and proves that our proposed algorithm

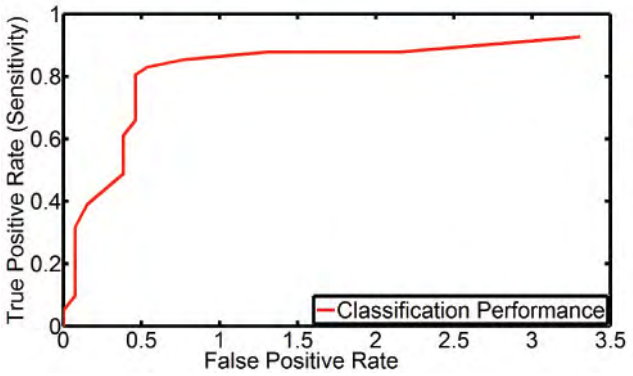

FIGURE 12. The receiver operating characteristic curve for the support vector machine classifier.

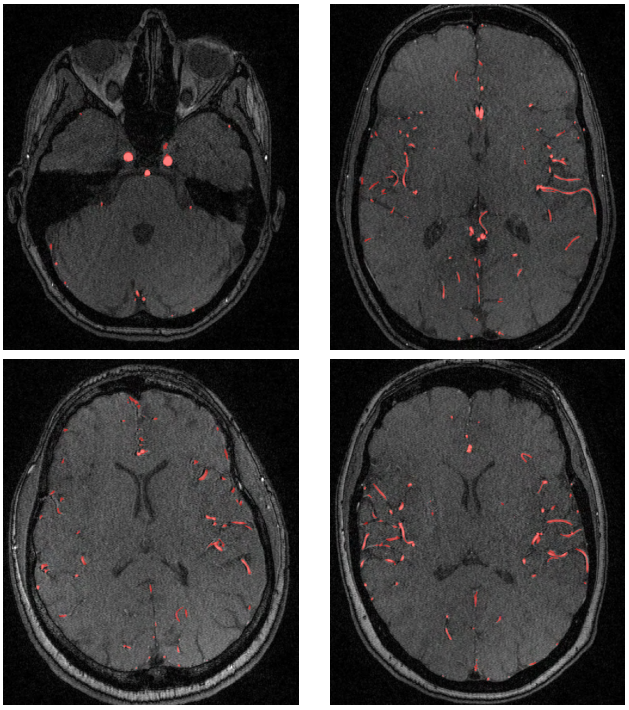

FIGURE 13. A 2D axial projection for the segmentation of different subjects from the validation data set using the proposed segmentation technique. The segmentation results are overlaid with red on the grey image.

provides a better segmentation over larger blood vessels, (at and below CoW), as well as smaller ones, (above CoW). The reported results for our approach used the SVM classifier with four-fold cross validation. To measure the statistical significance between the results of the proposed segmentation and the other techniques that used in the comparison, we used the paired t-test. The differences between the metrics means were found to be statistically significant as the corresponding p-values are below 0.0001. Figure 10 provides a 3D demonstration of the anatomical separation based on the coW. Moreover, in Table 2, we demonstrated the average execution time for each segmentation approach. The reported execution time is based on implementing the proposed approach on an Intel quad-core processor (3.2 GHz each) with 64 GB of memory and a 4 TB hard drive with RAID technology using Matlab. Finally, Figure 11 demonstrates 3D visualization of the extracted vascular system using the proposed segmentation framework. Another major metric, the receiver operating characteristic (ROC), is used to evaluate the robustness of our segmentation framework. The ROC tests the sensitivity of the segmentation results against the selection of the the classification threshold (operating point) by showing the relationship between the fractions of *TP* and *FP* rates at different threshold points as demonstrated in Figure 12.

In addition, the accuracy of the proposed approach was quantitatively validated using 30 data sets with a known manually segmented ground truth that was obtained by an MRA expert. Each data volume consists of a matrix of 696 $\times$ 768 with an in-plane spacing of 0.26 *mm* and was collected for patients who underwent stress analysis study. The average DC, AVVD, and BHD is 94.58%, 7.31%, and 2.85 *voxels* respectively. Figure 13 shows qualitative results for the validation data set, it shows a 2D axial projection from different subjects.

IV. CONCLUSION

In conclusion, the cerebral vascular diseases are threatening the life of millions around the world. The diagnosis of such diseases has been a challenge over the years and most physicians would agree that the most important step of recovery is having the right diagnosis. If the illness is precisely identified, most likely proper treatment will be done. Therefore, segmentation of the cerebrovascular structure is crucial since it helps in the diagnoses process, surgery planning, research, and monitoring. Moreover, the benefits of the segmentation of the cerebrovascular structure lay in its ability to improve the simulation of the blood flow and the visualization of the vessels in which each developed method solves a problem faced previously or triggers a specific region of the brain. This paper proposes a statistical approach that utilizes a voxel-wise classification based on determining probability models of voxel intensities in order to separate blood vessels from the background of each TOF-MRA slice. This is done by approximating the marginal empirical distribution of intensity probabilities with LCDG with alternate signs and utilizing EM-based techniques for linear combination of Gaussian approximation that are adapted for dealing with LCDGs.

REFERENCES

[1] J. Wang, S. Zhao, Z. Liu, Y. Tian, F. Duan, and Y. Pan, "An active contour model based on adaptive threshold for extraction of cerebral vascular structures," *Comput. Math. Methods Med.*, vol. 2016, pp. 1–9, Aug. 2016.

[2] X. Wang, E. Liu, Z. Wu, F. Zhai, Y.-C. Zhu, W. Shui, and M. Zhou, "Skeleton-based cerebrovascular quantitative analysis," *BMC Med. Imag.*, vol. 16, no. 1, p. 68, Dec. 2016.

[3] L. Wen, X. Wang, Z. Wu, M. Zhou, and J. S. Jin, "A novel statistical cerebrovascular segmentation algorithm with particle swarm optimization," *Neurocomputing*, vol. 148, pp. 569–577, Jan. 2015.

[4] N. D. Forkert, A. Schmidt-Richberg, J. Fiehler, T. Illies, D. Möller, D. Säring, H. Handels, and J. Ehrhardt, "3D cerebrovascular segmentation combining fuzzy vessel enhancement and level-sets with anisotropic energy weights," *Magn. Reson. Imag.*, vol. 31, no. 2, pp. 262–271, Feb. 2013.

[5] (2017). *Automatic Segmentation of Cerebrovascular Structures*. Accessed: Jan. 2, 2017. [Online]. Available: http://www.ucalgary.ca/miplab/node/8
[6] Y. Sato, S. Nakajima, N. Shiraga, H. Atsumi, S. Yoshida, T. Koller, G. Gerig, and R. Kikinis, "Three-dimensional multi-scale line filter for segmentation and visualization of curvilinear structures in medical images," *Med. Image Anal.*, vol. 2, no. 2, pp. 143–168, Jun. 1998.
[7] K. Krissian, G. Malandain, N. Ayache, R. Vaillant, and Y. Trousset, "Model based multiscale detection of 3D vessels," in *Proc. Workshop Biomed. Image Anal.*, Jun. 1998, pp. 202–210.
[8] F. Catté, P.-L. Lions, J.-M. Morel, and T. Coll, "Image selective smoothing and edge detection by nonlinear diffusion," *SIAM J. Numer. Anal.*, vol. 29, no. 1, pp. 182–193, Feb. 1992.
[9] C. Lacoste, G. Finet, and I. E. Magnin, "Coronary tree extraction from X-ray angiograms using marked point processes," in *Proc. 3rd IEEE Int. Symp. Biomed. Imag., Nano Macro*, Apr. 2006, pp. 157–160.
[10] M. A. Gülsün and H. Tek, "Robust vessel tree modeling," in *Proc. Int. Conf. Med. Image Comput. Comput.-Assisted Intervent.* Springer, 2008, pp. 602–611.
[11] M. Pechaud, R. Keriven, and G. Peyre, "Extraction of tubular structures over an orientation domain," in *Proc. IEEE Conf. Comput. Vis. Pattern Recognit. (CVPR)*, Jun. 2009, pp. 336–342.
[12] H. Li and A. Yezzi, "Vessels as 4-D curves: Global minimal 4-D paths to extract 3-D tubular surfaces and centerlines," *IEEE Trans. Med. Imag.*, vol. 26, no. 9, pp. 1213–1223, Sep. 2007.
[13] N. Zhu and A. C. Chung, "Minimum average-cost path for real time 3D coronary artery segmentation of CT images," in *Proc. Int. Conf. Med. Image Comput. Comput.-Assist. Intervent.* Springer, 2011, pp. 436–444.
[14] A. C. Jalba, M. H. F. Wilkinson, and J. B. T. M. Roerdink, "CPM: A deformable model for shape recovery and segmentation based on charged particles," *IEEE Trans. Pattern Anal. Mach. Intell.*, vol. 26, no. 10, pp. 1320–1335, Oct. 2004.
[15] L. M. Lorigo, O. D. Faugeras, W. E. L. Grimson, R. Keriven, R. Kikinis, A. Nabavi, and C.-F. Westin, "CURVES: Curve evolution for vessel segmentation," *Med. Image Anal.*, vol. 5, no. 3, pp. 195–206, Sep. 2001.
[16] T. Deschamps and L. D. Cohen, "Fast extraction of tubular and tree 3D surfaces with front propagation methods," in *Proc. 16th Int. Conf. Pattern Recognit.*, vol. 1, Aug. 2002, pp. 731–734.
[17] M. Holtzman-Gazit, R. Kimmel, N. Peled, and D. Goldsher, "Segmentation of thin structures in volumetric medical images," *IEEE Trans. Image Process.*, vol. 15, no. 2, pp. 354–363, Feb. 2006.
[18] R. Manniesing, B. K. Velthuis, M. S. van Leeuwen, I. C. van der Schaaf, P. J. van Laar, and W. J. Niessen, "Level set based cerebral vasculature segmentation and diameter quantification in CT angiography," *Med. Image Anal.*, vol. 10, no. 2, pp. 200–214, Apr. 2006.
[19] N. D. Forkert, D. Säring, T. Illies, J. Fiehler, J. Ehrhardt, H. Handels, and A. Schmidt-Richberg, "Direction-dependent level set segmentation of cerebrovascular structures," *Proc. SPIE, Med. Imag., Image Process.*, vol. 7962, Mar. 2011, Art. no. 79623S.
[20] M. Kass, A. Witkin, and D. Terzopoulos, "Snakes: Active contour models," *Int. J. Comput. Vis.*, vol. 1, no. 4, pp. 321–331, Jan. 1988.
[21] S. Zhao, M. Zhou, Y. Tian, P. Xu, Z. Wu, and Q. Deng, "Extraction of vessel networks based on multiview projection and phase field model," *Neurocomputing*, vol. 162, pp. 234–244, Aug. 2015.
[22] Y. Zhang, B. J. Matuszewski, L.-K. Shark, and C. J. Moore, "Medical image segmentation using new hybrid level-set method," in *Proc. 5th Int. Conf. Biomed. Visualization: Inf. Vis. Med. Biomed. Informat. (MEDIVIS)*, Jul. 2008, pp. 71–76.
[23] Q. Hong, Q. Li, B. Wang, Y. Li, J. Yao, K. Liu, and Q. Wu, "3D vasculature segmentation using localized hybrid level-set method," *Biomed. Eng. OnLine*, vol. 13, no. 1, p. 169, 2014.
[24] D. L. Wilson and J. A. Noble, "An adaptive segmentation algorithm for time-of-flight MRA data," *IEEE Trans. Med. Imag.*, vol. 18, no. 10, pp. 938–945, Oct. 1999.
[25] A. C. S. Chung and J. A. Noble, "Statistical 3D vessel segmentation using a Rician distribution," in *Proc. Int. Conf. Med. Image Comput. Comput.-Assist. Intervent.* Springer, 1999, pp. 82–89.
[26] A. R. Webb, *Statistical Pattern Recognition*. Hoboken, NJ, USA: Wiley, 2003.
[27] D. Nain, A. Yezzi, and G. Turk, "Vessel segmentation using a shape driven flow," in *Proc. Int. Conf. Med. Image Comput. Comput.-Assist. Intervent.* Springer, 2004, pp. 51–59.
[28] M. W. Law and A. C. Chung, "A deformable surface model for vascular segmentation," in *Proc. Int. Conf. Med. Image Comput. Comput.-Assist. Intervent.* Springer, 2009, pp. 59–67.
[29] R.-F. Cao, X.-C. Wang, Z.-K. Wu, M.-Q. Zhou, and X.-Y. Liu, "A parallel Markov cerebrovascular segmentation algorithm based on statistical model," *J. Comput. Sci. Technol.*, vol. 31, no. 2, pp. 400–416, Mar. 2016.
[30] T. Woźniak, M. Strzelecki, A. Majos, and L. Stefańczyk, "3D vascular tree segmentation using a multiscale vesselness function and a level set approach," *Biocybern. Biomed. Eng.*, vol. 37, no. 1, pp. 66–77, 2017.
[31] S. Zhao, Y. Tian, X. Wang, P. Xu, Q. Deng, and M. Zhou, "Vascular extraction using MRA statistics and gradient information," *Math. Problems Eng.*, vol. 2018, pp. 1–8, Feb. 2018.
[32] H. Kandil, A. Soliman, F. Taher, A. Mahmoud, A. Elmaghraby, and A. El-Baz, "Using 3-D CNNs and local blood flow information to segment cerebral vasculature," in *Proc. IEEE ISSPIT*, Dec. 2018, pp. 701–705.
[33] M. Livne, J. Rieger, O. U. Aydin, A. A. Taha, E. M. Akay, T. Kossen, J. Sobesky, J. D. Kelleher, K. Hildebrand, D. Frey, and V. I. Madai, "A U-net deep learning framework for high performance vessel segmentation in patients with cerebrovascular disease," *Frontiers Neurosci.*, vol. 13, Feb. 2019.
[34] N. J. Tustison, B. B. Avants, P. A. Cook, Y. Zheng, A. Egan, P. A. Yushkevich, and J. C. Gee, "N4ITK: Improved N3 bias correction," *IEEE Trans. Med. Imag.*, vol. 29, no. 6, pp. 1310–1320, Jun. 2010.
[35] C. Bouman and K. Sauer, "A generalized Gaussian image model for edge-preserving MAP estimation," *IEEE Trans. Image Process.*, vol. 2, no. 3, pp. 296–310, Jul. 1993.
[36] J. Besag, "On the statistical analysis of dirty pictures," *J. Roy. Stat. Soc., B Methodol.*, vol. 48, no. 3, pp. 259–279, Jul. 1986.
[37] A. A. Farag, A. S. El-Baz, and G. Gimel'farb, "Precise segmentation of multimodal images," *IEEE Trans. Image Process.*, vol. 15, no. 4, pp. 952–968, Apr. 2006.
[38] A. El-Baz, A. Farag, and G. Gimelfarb, "Cerebrovascular segmentation by accurate probabilistic modeling of TOF-MRA images," in *Proc. Scand. Conf. Image Anal.* Springer, 2005, pp. 1128–1137.
[39] A. Soliman, F. Khalifa, A. Alansary, G. Gimel'farb, and A. El-Baz, "Performance evaluation of an automatic MGRF-based lung segmentation approach," in *Proc. AIP Conf.*, 2013, vol. 1559, no. 1, pp. 323–332.
[40] G. Gerig, M. Jomier, and M. Chakos, "Valmet: A new validation tool for assessing and improving 3d object segmentation," in *Proc. Int. Conf. Med. Image Comput. Comput.-Assist. Intervent.* Springer, 2001, pp. 516–523.

FATMA TAHER (Member, IEEE) received the Ph.D. degree from the Khalifa University of Science, Technology and Research, United Arab Emirates, in 2014. She is currently the Assistant Dean of the College of Technological Innovation, Zayed University, Dubai, United Arab Emirates. She has published more than 40 articles in international journals and conferences. Her research interests are in the areas of signal and image processing, pattern recognition, deep learning, machine learning, artificial intelligence, medical image analysis, especially in detecting of the cancerous cells, kidney transplant, and autism. In addition to that, her researches are watermarking, remote sensing, and satellite images. She served as a member of the steering, organizing, and technical program committees of many international conferences. She has received many distinguished awards, such as the Best Paper Award of the first prize in the Ph.D. Forum of the 20th IEEE International Conference on Electronics, Circuits, and Systems (ICECS), the Ph.D. Forum, December 2013. And recently, she received the UAE Pioneers Award as the first UAE to create a computer-aided diagnosis system for early lung cancer detection based on the sputum color image analysis, awarded by H. H. Sheik Mohammed Bin Rashed Al Maktoum, November 2015. In addition to that, she received the Innovation Award at the 2016 Emirati Women Awards by H. H. Sheik Ahmed Bin Saeed Al Maktoum. She was the Chairman of Civil Aviation Authority and a Patron of Dubai Quality Group and L'Oréal-UNESCO for Women in Science Middle East Fellowship 2017. She is the Vice Chair of the IEEE UAE section and the Chair of the Education Committee in British Society, United Arab Emirates. She has served on many editorial and reviewing boards of international journals and conferences.

AHMED SOLIMAN (Member, IEEE) received the Ph.D. degree in electrical engineering from the Electrical and Computer Engineering Department, University of Louisville, USA, in 2016. He is currently working as a Postdoctoral Research Associate at the Bioengineering Department, University of Louisville. He is working on the development of new image processing-based techniques for early detection of cancer, transplant rejection, lung injury, autism spectrum disorder, and other healthcare issues. He has extensive experience in computer modeling, medical image analysis, and computational imaging, including nine years of experience in using and applying computer-aided design in research.

HEBA KANDIL (Member, IEEE) received the B.Sc. and M.S. degrees in computer science from Mansoura University, Mansoura, Egypt. In August 2016, she joined the Bioimaging Laboratory, University of Louisville, Louisville, KY, USA, as a Ph.D. Student, where she is currently pursuing the Ph.D. degree from the Computer Science and Computer Engineering Department. Her current research is focused on developing new computer assisted diagnostic systems for diagnosing severe diseases correlated with cerebrovascular changes in human beings.

ALI MAHMOUD (Member, IEEE) received the B.S. and M.S. degrees in electrical engineering from Alexandria University, Egypt, in 2005 and 2009, respectively, and the Ph.D. degree in electrical engineering from the University of Louisville, Louisville, USA, in 2014. He is currently working as a Postdoctoral Research Associate at the Bioengineering Department, University of Louisville. His research interests include computer vision and image processing, object detection and tracking, medical imaging, and facial biometrics.

AHMED SHALABY (Member, IEEE) received the B.S. and M.S. degrees in electrical engineering from Alexandria University, Egypt, in 2003 and 2009, respectively, and the Ph.D. degree in electrical engineering from the University of Louisville, Louisville, USA, in 2014. He is currently working as a Postdoctoral Research Associate at the Bioengineering Department, University of Louisville. His research interests include computer vision and image processing, object detection and tracking, medical imaging, and facial biometrics.

GEORGY GIMEL'FARB (Member, IEEE) received the Candidate of Engineering Sciences degree (equivalent to the Ph.D.) from the Academy of Sciences of Ukrainian SSR, in 1969, and the advanced Doctor of Engineering Sciences degree from the Higher Certifying Commission of the USSR, in 1991. After the long-term work at the Glushkov's Institute of Cybernetics of the National Ukrainian Academy of Sciences, he joined The University of Auckland, New Zealand, in 1997, where he is currently a Professor and the Co-Director of the Intelligent Vision Systems Laboratory. His research interests include statistical pattern recognition, probabilistic image modeling, texture analysis in remotely sensed and medical images, and computational stereo vision. He was a recipient of the prestigious State Premium of Ukraine in Science and Technology, in 1997, for fundamental and applied research results in image and signal recognition and development on their basis of intelligent information technologies and systems.

AYMAN EL-BAZ (Senior Member, IEEE) received the bachelor's and master's degrees in electrical engineering in 1997 and 2001, respectively, and the Ph.D. degree in electrical engineering from the University of Louisville, in 2006. He is currently a Professor, an University Scholar, and the Chair of the Bioengineering Department at the University of Louisville, KY, USA. He has 15 years of hands-on experience in the fields of bio-imaging modeling and non-invasive computer-assisted diagnosis systems. He has authored or coauthored more than 450 technical articles. In 2009, he was named as a Coulter Fellow for his contributions to the field of biomedical translational research.